IEEE Access
Multidisciplinary ⋮ Rapid Review ⋮ Open Access Journal

Received December 26, 2021, accepted January 6, 2022, date of publication January 11, 2022, date of current version January 20, 2022.

Digital Object Identifier 10.1109/ACCESS.2022.3141865

Performance Analysis of Short Packets in NOMA VLC Systems

GIANG N. TRAN, (Graduate Student Member, IEEE), AND SUNGHWAN KIM, (Member, IEEE)

Department of Electrical, Electronic, and Computer Engineering, University of Ulsan, Ulsan 44610, South Korea

Corresponding author: Sunghwan Kim (sungkim@ulsan.ac.kr)

This work was supported by the National Research Foundation of Korea through the Research Program under Grant NRF-2019R1A2C1005920.

ABSTRACT In this paper, we propose a theoretical framework for analyzing the performance of the short-packet communication (SPC) in a downlink non-orthogonal multiple access (NOMA) visible light communication (VLC) system in which one light emitting diode (LED) communicates with two single-photodiode users. The analytical expression of the block error rate (BLER) is approximated by Gaussian-Chebyshev quadrature method, based on which the reliability, throughput, and latency expressions are deduced. Further, we jointly optimize power allocation coefficients and transmission rates to maximize sum throughput of the SPC-NOMA VLC system. The numerical results show that (i) our proposed system well satisfies the stringent requirements of the ultra-reliable and low latency communication (URLLC) at signal-to-noise ratio (SNR) larger than 130 dB; (ii) SPC-NOMA VLC systems outperform SPC- orthogonal multiple access (OMA) VLC systems in terms of reliability, latency, and throughput; (iii) the impacts of block-length, power allocation coefficients, transmission rates, and LED semi-angle are examined.

INDEX TERMS Short packet communication (SPC), non-orthogonal multiple access (NOMA), visible light communication (VLC), ultra-reliable and low latency communication (URLLC).

I. INTRODUCTION

Driven by the ever-increasing penetration of the digitization era in the globe, wireless data traffic with high network capacity demand is expected to substantially increase [1]. Ongoing research on future wireless networks that could plausibly satisfy future client data needs has consistently intensified [2]–[4]. Along with the fifth-generation (5G) technologies, visible light communication (VLC) has attracted considerable attention for high-speed and short-range wireless communications due to its many inherent advantages such as license-free spectrum, low-cost front-ends, high security, and strong immunity to electromagnetic interference [3], [4]. To be considered as a high-capacity wireless broadband technology, the developed VLC systems can effectively support low-latency communications that are pivotal to ensure real-time functionality in interactive communications of machines in industrial automation applications [5] and support multiple users with simultaneous network access [6].

5G technology is expected to satisfy the ultra-reliable (i.e., $>$ 99.999%) and low latency (sub-millisecond) communication (URLLC) requirement for the real time applications and Internet-of-Things (IoTs) ones (e.g., telesurgery, factory automation, machine-to-machine communication, and intelligent transportation). In [7], the domain knowledge of communications and networking was integrated into emerging deep learning techniques to guarantee the quality of services (QoS) constraints, and improved the performance of networks in terms of delay, reliability, and jitter, since transmission delay and reliability are two key parameters for the URLLC applications. To end this, the short packet communication (SPC) was introduced as a potential method in 5G and beyond [8], [9]. The authors of [10] showed that the Shannon capacity of the infinite block-length cannot be applied for the finite block-length communication in SPC. Alternatively, the achievable rate of the SPC was represented in term of the Shannon capacity, block-length, and block error rate (BLER) of the model, and the length of the block was

The associate editor coordinating the review of this manuscript and approving it for publication was Donatella Darsena.

longer than that of the actual data [11], [12]. The benefits of the SPC have been widely studied on different communication systems, e.g., quasi-static multiple-input multiple-output [13], latency-critical packet scheduling [14]. However, to the best of our knowledge, the application and investigation of SPC for VLC systems to reduce transmission latency are still questioned.

Second, the conventional orthogonal multiple access (OMA) (e.g., frequency division multiple access (FDMA), time division multiple access (TDMA), and code division multiple access) has limitations for massive connectivity due to the rareness of resources (i.e., time slots, frequencies, and bandwidth) [11], [12]. As a solution of this gap, non-orthogonal multiple access (NOMA) has recently been developed as an auspicious candidate technology for ability to serve multiple users simultaneously in the same resource block (i.e., time slot, subcarrier, and spreading code) in power domain [15]. In NOMA, higher power coefficients are allocated to the message signal of a poor-channel user, and lower power coefficients are allocated to the message signal of a good-channel user. Therefore, the performance of NOMA systems has been studied in various contexts, such as broadcast channels [16], full-duplex communications [17], physical layer security [18], multiple-input multiple-output systems [19], cognitive radio [20], and radio-frequency energy harvesting [21]. By utilizing NOMA, higher power was allocated to the message signal for the poor-channel users to ensure the achievable target rates at these users, thus balancing the network throughput and user fairness [22]. The necessary and sufficient conditions for the power ranges for each user in the two-user NOMA system were determined with the error floor limitation of the symbol constellation detection of successive interference cancellation (SIC) operation in [23]. Moreover, the authors of [24] proposed a framework for power ranges and optimum power allocation for NOMA systems with an arbitrary number of users. Also, the implementation of NOMA in the wireless communication provided higher flexibility and more efficient use of spectrum and energy, and overloading spectrum caused by multiplexing users was solved [25]. The implement of NOMA in VLC systems can provide efficient resource utilization to support a huge number of high-speed devices in indoor environments. Few studies about the implementation of NOMA in VLC systems have confirmed that NOMA is a potential candidate for high-speed VLC systems. For instance, the authors of [26] proposed the NOMA based directional light fidelity (LiFi) system in which visible light was used in the downlink and infrared light was used in uplink to improve energy efficiency and support for high-speed IoT devices. The performance of NOMA and orthogonal FDMA was compared in a VLC system with illumination constraints, and its outperformance was shown in [25]. A prior theoretical study on the performance evaluation of NOMA in a multi-user VLC system was presented in [27]. The authors of [28] proposed a power allocation algorithm based on the user level and subcarrier-level power allocation to obtain the maximum sum of data rate and the minimum subcarrier loss rate of the OFDM based NOMA VLC system. It is highlighted that due to the fundamental differences between the VLC channel and the radio frequency (RF) channel, applying NOMA to VLC required careful reconsiderations [27], [29].

To overcome the barriers and accommodate demand on URLLC as well as provide massive connectivity, the combination of NOMA and SPC has been studied in the field of RF systems [12], [13], [16]. The SPC can be employed in VLC systems by utilizing Hermitian symmetry and adding direct current (DC) bias. However, to the best of our knowledge, few researches had been studied to explore the effectiveness of the NOMA VLC system. The aforementioned works have mainly discussed on the achievable rate of the NOMA VLC systems while the reliability and latency were not mentioned [6], [27], [29]. This brings a new exploration of a coupled SPC-NOMA scheme for the VLC system of multiple users and URLLC. This paper is the first study on the SPC-NOMA VLC with the analyses for the reliability, latency, and throughput. The contributions of this paper are summarized as below.

- We, for the first time, propose the SPC in NOMA VLC systems to increase reliability and reduce latency. The results of the proposed SPC-NOMA VLC system show that the reliability increases slowly at low SNR; however, it increases quickly at the medium and high SNR.
- The analytical expression of the BLER are approximated by Gaussian-Chebyshev quadrature method, and then the approximate expressions for reliability, latency, and throughput are also carried out.
- SPC and long-packet communication (LPC) in NOMA VLC systems are evaluated in terms of reliability and latency. The satisfaction of the SPC-NOMA VLC system for URLLC applications is presented in the comparison to the LPC-NOMA VLC system.
- The performance of the SPC-NOMA VLC system and SPC-OMA VLC system is analyzed in terms of reliability, latency, and throughput.
- The effect of choosing the LEDs with various semi-angles on the sum throughput is evaluated for the SPC-NOMA VLC system.
- The optimal values of transmission rates and power allocation coefficients to maximize the sum throughput of the SPC-NOMA VLC system are determined by the numerical search method.

The rest of this paper is organised as follows. The preliminaries of the SPC in the RF system, and both NOMA and OMA in the VLC system are introduced in Section II. In Section III, the system model is described, and the performance evaluation of the SPC in both NOMA VLC and OMA VLC systems and the optimization design for the throughput of the SPC-NOMA VLC are presented. Section IV shows the simulation results and the comparison of the LPC to the SPC in the NOMA VLC system, and the comparison of the SPC-NOMA VLC to the OMA VLC schemes. Finally,

TABLE 1. Table of symbols and notations.

Notation	Description
$\|\cdot\|$	Absolute value
$E\{\cdot\}$	Expectation operator
$Q(\cdot)$	Gaussian Q-function
P	Electrical power of the message signal
$f_X(\cdot)$	Probability density function (PDF)
$F_X(\cdot)$	Cumulative distribution function (CDF)
U_i	User i
h_i	Channel gain between the transmitter and user i
μ_i	Additive white Gaussian noise at user i
σ_i^2	Variance of the noise at user i
γ_{Tx}	Transmitted signal-to-noise ratio (SNR)
γ_i	Signal-to-noise-plus-interference ratio (SINR) at user i
a_i	Power allocation coefficient to user i
k_i	Number of information bits for user i
N_i	Block-length for user i
R_i	Transmission rate for user i
ε_i	Block error rate (BLER) at user i
$\bar{\varepsilon}_i$	Average BLER at user i
T_i	Throughput at user i

Section V is conclusion of the paper. For clarity, we summarize the main symbols and notations in Table 1.

II. BACKGROUND

A. SPC IN RF SYSTEMS

In the RF system, the message signal x_s of the SPC is directly transmitted from the source to the destination. The signal at the receiver is presented as

$$y = Px_s|h|^2 + \mu_D, \tag{1}$$

where $|h|$ is magnitude of the channel gain, P is the electrical power of the message signal, and μ_D is the additive white Gaussian noise (AWGN) with the variance σ^2. In the SPC, each packet is transmitted in message signals. Each packet contains the information bits and addition bits (or metadata) for correct functioning [11]. The BLER of the detection at the receiver is approximated by [8, Eq. (59)], [30, Eq. (11)]

$$\varepsilon \approx Q\left(\frac{C(\gamma) - R}{\sqrt{V(\gamma)/N}}\right), \tag{2}$$

where $\gamma = P|h|^2/\sigma^2$ is the received signal-to-noise ratio (SNR), N is the block-length ($N \geq 100$), $R = k/N$ is the transmission rate, k is the number of information bits in a packet, $C(\gamma) = \log_2(1+\gamma)$ is the Shannon capacity, and $V(\gamma) = \left(1 - (1+\gamma)^{-2}\right)\left(\log_2 e\right)^2$ is the channel dispersion, and $Q(.)$ is Gaussian Q-function, with $Q(x) = \int_x^\infty e^{-t^2/2}\,dt$.

The average BLER is calculated by

$$\begin{aligned}\bar{\varepsilon} &\approx E\left\{Q\left(\frac{C(\gamma) - R}{\sqrt{V(\gamma)/N}}\right)\right\} \\ &= \int_{-\infty}^{\infty} Q\left(\frac{C(\gamma) - R}{\sqrt{V(\gamma)/N}}\right) f_\gamma(x)\,dx,\end{aligned} \tag{3}$$

where $E\{.\}$ is expectation, and $E\{X\} = \int_{-\infty}^{\infty} x f_X(x)\,dx$.

B. NOMA VLC

The principle of NOMA schemes is based on the channel quality, shown in Fig. 1. We consider that two users are scheduled in one cluster and served in a resource block.[1] We define that the far user U_1 has lower channel gain, and the near user U_2 has higher channel gain. The message signals for users are superposed in the power domain. The poorer the user's channel is, the higher power coefficient is allocated. After Hermitian symmetry and adding DC bias [6], [27], [29], the superposed signal at one LED is given by

$$x_{\text{LED}} = \sqrt{a_1 P}s_1 + \sqrt{a_2 P}s_2 + V_{\text{DC}}, \tag{4}$$

where V_{DC} is the DC bias added for non-negative unipolar signal, s_1 and s_2 are the intended message signals for U_1 and U_2, and a_1 and a_2 are the power coefficients allocated to the message signals of U_1 and U_2. Total power allocation coefficients must satisfy: $a_1 + a_2 = 1$ and $a_1 \geq a_2$.

At U_1 ($i \in \{1, 2\}$), DC bias is eliminated, and the received signal is given by

$$y_i = h_i\left(\sqrt{a_1 P}s_1 + \sqrt{a_2 P}s_2\right) + \mu_i, \tag{5}$$

where μ_i is the zero-mean real-valued AWGN with the variance σ_i^2 and h_i is the channel gain between the LED and U_i. After optical-to-electrical conversion, the signal processing is presented as following.

At U_1, the SIC is not performed, and the intended signal is directly decoded. The SINR is given by

$$\gamma_{11} = \frac{a_1 h_1^2}{a_2 h_1^2 + 1/\gamma_{\text{Tx}}}, \tag{6}$$

where $\gamma_{\text{Tx}} = \frac{P}{\sigma_i^2}$ is the transmitted SNR.

At U_2, the SIC is performed to remove the interference of the message for U_1, and the message for U_1 is treated as the interference. The SINR of the intended message for U_2 at U_1 is given by

$$\gamma_{21} = \frac{a_1 h_2^2}{a_2 h_2^2 + 1/\gamma_{\text{Tx}}}. \tag{7}$$

The SINR of the own signal for U_2 is given by

$$\gamma_{22} = \frac{a_2 h_2^2}{a_1 h_2^2 \delta_{21} + 1/\gamma_{\text{Tx}}}, \tag{8}$$

where $\delta_{21} \in [0, 1]$ is the imperfect SIC factor.[2] In this paper, for the goal of evaluating optimal system performance, we consider $\delta_{21} = 0$.

[1] When there are more than two users in the system, users are sorted and paired, and the hybrid NOMA/OMA is used to support multiple user pairs. The power domain NOMA multiplexes two users of each pair. User pairs are multiplexed by the OMA scheme. When the number of users is odd, users are sorted and paired, and the remaining unpairing one is supported by the separate power and resource block [31].

[2] In practice, due to the imperfect SIC circuit design and error propagation, the operation of SIC may result in the residual interference, which leads to the degradation of system performance.

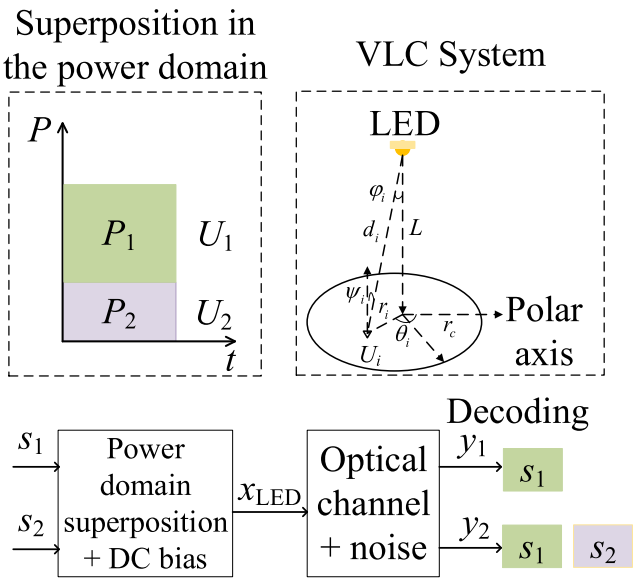

FIGURE 1. Principle of the two-user NOMA and VLC systems.

C. OMA VLC

In this paper, we consider that TDMA is adopted to serve users in the orthogonal time resource. The transmitted signal for U_i at one LED is given by

$$x_i = \sqrt{a_i P} s_i + V_{\mathrm{DC}}. \tag{9}$$

Equation (9) assumes that there is no interference at U_i caused by other users in the OMA VLC system. After removing DC bias, the received signal at U_i is presented by

$$y_i = \sqrt{a_i P} h_i s_i + \mu_i. \tag{10}$$

Then, the received SNR at U_i is given by

$$\gamma_i^{\mathrm{o}} = \frac{a_i P h_i^2}{\sigma_i^2} = a_i h_i^2 \gamma_{Tx}. \tag{11}$$

D. DISTRIBUTION FUNCTION OF THE RECEIVED SNR

The power allocation strategy for all users at the transmitter is based on the knowledge of the channel quality. In the two-user NOMA system, the channel gain quality is assumed to be ordered as

$$h_1 \le h_2. \tag{12}$$

The positions of receivers are assumed to be uniformly distributed within the circular area under the LED. The cell radius is denoted by r_{c}. The vertical distance between the LED and users on the circle plane is denoted by L. In the polar coordinate system, the position of U_i is presented by (r_i, θ_i), where r_i is the horizontal distance from the LED to the receiver and θ_i is the polar angle from the polar axis. The channel gain between U_i and the LED is given by

$$h_i = \frac{(m+1) A R_p}{2\pi d_i^2} \cos^m(\phi_i) T(\psi_i) g(\psi_i) \cos(\psi_i), \tag{13}$$

where Lambertian radiation pattern is given by $m = -\ln(2)/\ln(\cos(\Phi_{1/2}))$; $\Phi_{1/2}$ is the semi-angle of the LED; Ψ_{FOV} is the field-of-view (FOV) semi-angle of the photodiode (PD) at each receiver; A is detection area of the PD; R_{p} is the responsivity of the PD; d_i is the Euclidean distance between the receiver and the LED; ψ_i is the angle of irradiance; ψ_i is the angle of incidence; $T(\psi_i)$ is the gain of optical filter at the receiver; and $g(\psi_i)$ is the gain of the optical concentrator at the receiver, given by

$$g(\psi_i) = \begin{cases} \dfrac{n^2}{\sin^2(\Psi_{\mathrm{FOV}})}, & 0 \le \psi_i \le \Phi_{\mathrm{FOV}}, \\ 0, & \psi_i > \Phi_{\mathrm{FOV}}, \end{cases} \tag{14}$$

where n is the refractive index of the optical concentrator, $n \in [1, 2]$.

From Fig. 1, the Euclidian distance between the LED and U_i, the angle of irradiance, and the angle of incidence are calculated by $d_i = \sqrt{r_i^2 + L^2}$, $\cos(\phi_i) = L/\sqrt{r_i^2 + L^2}$, and $\cos\psi_i = L/\sqrt{d_i^2 + L^2}$, respectively. With the uniform distribution, the probability density function (PDF) of a location in a circle is given by $f_{r_i}(r) = 2r/r_{\mathrm{c}}^2$.

According to [29], the unordered PDF of received SNR at U_i is obtained by using the method of transformation and the change of variable method [32, Chap. 6] as

$$f_{\gamma_i}(x) = \frac{1}{r_{\mathrm{c}}^2} \frac{1}{m+3} \left(\mathcal{C}(m+1) L^{m+1}\right)^{\frac{2}{m+3}} \left(\frac{1}{\gamma_{\mathrm{Tx}}}\right)^{-\frac{1}{m+3}} \times x^{-\frac{m+4}{m+3}}, \tag{15}$$

where $\mathcal{C} = \frac{1}{2\pi} A T(\psi_i) g(\psi_i)$ and $\gamma_i = \gamma_{\mathrm{Tx}} h_i^2$. Since $h_i^2 \in [h_{\min}^2, h_{\max}^2]$, $h_{\min}^2 = \left(\mathcal{C}(m+1)L^{m+1}\right)^2 / \left(r_{\mathrm{c}}^2 + L^2\right)^{(m+3)}$, and $h_{\max}^2 = \left(\mathcal{C}(m+1)L^{m+1}\right)^2 / L^{2(m+3)}$, then $\gamma_i \in [\gamma_{\min}, \gamma_{\max}] = [\gamma_{\mathrm{Tx}} h_{\min}^2, \gamma_{\mathrm{Tx}} h_{\max}^2]$. The cumulative distribution function (CDF) of the received SNR at U_i is obtained by integrating (15) with respect to $x \in [\gamma_{\min}, \gamma_{\max}]$. The unordered CDF of the received SNR is given as

$$F_{\gamma_i}^{\gamma}(x) = \frac{1}{r_{\mathrm{c}}^2} \frac{1}{m+3} \left(\mathcal{C}(m+1)L^{m+1}\right)^{\frac{2}{m+3}} \times \left(\frac{1}{\gamma_{\mathrm{Tx}}}\right)^{-\frac{1}{m+3}} x^{-\frac{1}{m+3}} + \frac{L^2}{r_{\mathrm{c}}^2} + 1. \tag{16}$$

Since the channel quality is ordered for the power allocation, the ordered statistics [29], [32, Chap. 6], [33] are considered in this paper. The ordered CDF of the received SINR at U_i is presented by

$$\begin{aligned} F_{\gamma_i}(x) &= \sum_{\hat{j}=i}^{2} \frac{2!}{(2-\hat{j})!\hat{j}!} \left(F_{\gamma_i}^{\gamma}(x)\right)^{\hat{j}} \left(1 - F_{\gamma_i}^{\gamma}(x)\right)^{2-\hat{j}} \\ &= \sum_{\hat{j}=i}^{2} \frac{2!}{(2-\hat{j})!\hat{j}!} \left(-\omega x^{-\frac{1}{m+3}} + \frac{L^2}{r_{\mathrm{c}}^2} + 1\right)^{\hat{j}} \\ &\quad \times \left(\omega x^{-\frac{1}{m+3}} - \frac{L^2}{r_{\mathrm{c}}^2}\right)^{2-\hat{j}}, \end{aligned} \tag{17}$$

where $\omega = \frac{1}{r_{\mathrm{c}}^2} \left(\mathcal{C}(m+1)L^{m+1}\right)^{\frac{2}{m+3}} \left(\frac{1}{\gamma_{\mathrm{Tx}}}\right)^{-\frac{1}{m+3}}$.

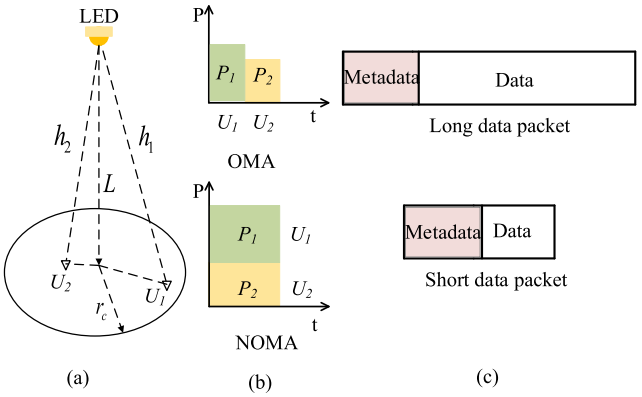

FIGURE 2. Illustration of the SPC-LPC in NOMA and OMA VLC system. (a) Proposed overall system model with VLC. (b) NOMA and OMA transmission. (c) SPC versus LPC.

III. SYSTEM MODEL AND PERFORMANCE EVALUATION

A. SYSTEM MODEL

In this work, we consider the transmission in a downlink broadcast channel for the indoor environment. To effectively present the system performance, we choose a general VLC system consisting of one LED and two users. The system model is depicted in Fig. 2. The LED is located on the ceiling to serve two single-photodiode users. The channel is static or quasi-static, so that the channel state is not changed during the transmission. We assume that the channel state information (CSI) is perfectly known at the LED and users. The users are uniformly distributed in a circle area. At the receiver side, the received signals include both line-of-sight (LOS) components and diffuse components caused by the reflections on the interior surfaces, such as the ceiling, floor, and walls. The authors of [6] have reported that the power of the LOS components is much higher than that of the non-LOS components. Therefore, we consider the LOS link from the LEDs to users. In the OMA scheme, TDMA is chosen to serve two users in orthogonal time resources. In the NOMA scheme, two users are served simultaneously, and perfect SIC is used at the poorer channel user for the signal detection. We denote the far user as the U_1 with the channel gain h_1, and the near user is denoted by U_2 with the channel gain h_2, $(h_1 \leq h_2)$. The noise is real value AWGN with zero mean and unit variance $\sigma^2 = 1$.

B. THE SPC IN VLC SYSTEMS

In VLC systems, the transmitted signals are required to be real and non-negative for the intensity modulation and direct detection (IM/DD). When employing the SPC in VLC systems, Hermitian symmetry is used to get real signal, and then the DC bias is added at the LED to guarantee non-negative signals for transmission. The message signal at the LED is presented by

$$x_{\text{LED}} = \sqrt{P} x_{\text{s}} + V_{\text{DC}}. \tag{18}$$

After optical-to-electrical conversion and removing DC bias at the receiver, the received signal is given as

$$y = \sqrt{P} h x_{\text{s}} + \mu_0, \tag{19}$$

where μ_0 is zero mean real-valued AWGN with σ_0^2. After removing DC bias at the receiver, the SNR at U_i is given by

$$\gamma_i = \gamma_{\text{Tx}} h_i^2. \tag{20}$$

Due to the utilization of Hermitian symmetry, the scaling factor 0.5 is multiplied with the Shannon capacity $C(\gamma_i)$ and channel dispersion $V(\gamma_i)$ in the expression of the BLER of the SPC in the VLC system. The BLER of the SPC in the VLC system at U_i $(i \in \{1, 2\})$ is approximated by

$$\varepsilon_i \approx Q\left(\frac{0.5\, C(\gamma_i) - R_i}{\sqrt{0.5\, V(\gamma_i)/N_i}}\right), \tag{21}$$

where N_i, k_i, and R_i are block-length, number of information bits allocated to U_i, and transmission rate at U_i, respectively.

The average BLER of the SPC in the VLC system is approximated by

$$\begin{aligned}\bar{\varepsilon}_i &\approx E\left\{Q\left(\frac{0.5\, C(\gamma_i) - R_i}{\sqrt{0.5\, V(\gamma_i)/N_i}}\right)\right\} \\ &= \int_0^{\infty} Q\left(\frac{0.5\, C(\gamma_i) - R_i}{\sqrt{0.5\, V(\gamma_i)/N_i}}\right) f_{\gamma_i}(x)dx. \end{aligned} \tag{22}$$

Since the received SNR is limited in the circle area under the LED, then $\gamma \in [\gamma_{\min}, \gamma_{\max}]$. The average BLER is approximated by

$$\bar{\varepsilon}_i \approx \int_{\gamma_{i,\min}}^{\gamma_{i,\max}} Q\left(\frac{0.5\, C(\gamma_i) - R_i}{\sqrt{0.5\, V(\gamma_i)/N_i}}\right) f_{\gamma_i}(x)dx. \tag{23}$$

Using partial integral, (23) is expressed by

$$\begin{aligned}\bar{\varepsilon}_i = {} & F_{\gamma_i}(x) Q\left(\frac{\log_2(1+x) - 2R_i}{\sqrt{2\left(1 - \frac{1}{(1+x)^2}\right)(\log_2 e)^2/N_i}}\right)\Bigg|_{\gamma_{i,\min}}^{\gamma_{i,\max}} \\ & - \int_{\gamma_{i,\min}}^{\gamma_{i,\max}} F_{\gamma_i}(x)\zeta(x)dx, \end{aligned} \tag{24}$$

where $F_{\gamma_i}(x)$ is cumulative distribution function (CDF) of the variable x, and $\zeta(x)$ is the first order derivative of the BLER expression, and $\frac{dQ(f(x))}{dx} = -\frac{1}{\sqrt{2\pi}}\frac{df(x)}{dx}e^{-f(x)^2/2}$. The function $\zeta(x)$ is expressed by

$$\begin{aligned}\zeta(x) = -\frac{1}{\sqrt{2\pi}} & \left(\frac{\sqrt{N_i/2}}{(1+x)\sqrt{\left(1 - \frac{1}{(1+x)^2}\right)}}\right. \\ & \left. - \frac{\sqrt{N_i/2}\left(\log_2(1+x) - 2R_i\right)}{\log_2 e \left(1 - \frac{1}{(1+x)^2}\right)^{3/2}(1+x)^3}\right) \\ & \times e^{-\frac{1}{2}\left(\frac{\log_2(1+x) - 2R_i}{\sqrt{2\left(1 - \frac{1}{(1+x)^2}\right)(\log_2 e)^2/N_i}}\right)^2}. \end{aligned} \tag{25}$$

It is complicated to derive the close-form expression of the remaining integral in (24). The average

BLER is approximated by using the Gaussian-Chebyshev quadrature method as [34, Table 25.4]

$$\begin{aligned}\bar{\varepsilon}_i &\triangleq f\left(\gamma_{i,\max}, \gamma_{i,\min}, N_i, R_i\right)\\ &= Q\left(\frac{0.5\,C\left(\gamma_{i,\max}\right)-R_i}{\sqrt{0.5\,V\left(\gamma_{i,\max}\right)/N_i}}\right)F_{\gamma_i}\left(\gamma_{i,\max}\right)\\ &\quad -Q\left(\frac{0.5\,C\left(\gamma_{i,\min}\right)-R_i}{\sqrt{0.5\,V\left(\gamma_{i,\min}\right)/N_i}}\right)F_{\gamma_i}\left(\gamma_{i,\min}\right)\\ &\quad -\nu_i\sum_{v=1}^{\bar{V}}\frac{\pi}{\bar{V}}\sqrt{1-\cos^2\left(\frac{(2v-1)\pi}{2\bar{V}}\right)}\\ &\quad \times F_{\gamma_i}\left(\nu_i\cos\left(\frac{(2v-1)\pi}{2\bar{V}}\right)+\vartheta_i\right)\\ &\quad \times g\left(\nu_i\cos\left(\frac{(2v-1)\pi}{2\bar{V}}\right)+\vartheta_i\right),\end{aligned} \tag{26}$$

where $\bar{V}$ is the complexity-accuracy trade-off parameter, $\nu_i = \frac{\gamma_{i,\max}-\gamma_{i,\min}}{2}$, and $\vartheta_i = \frac{\gamma_{i,\max}+\gamma_{i,\min}}{2}$.

Reliability at U_i is the probability that the packet is correctly detected, given by

$$\chi = (1-\varepsilon_i)100\%. \tag{27}$$

Throughput at U_i is the number of correctly determined information bits at the receiver per transmission, presented by

$$T_i = \frac{N_i}{N}R_i(1-\varepsilon_i). \tag{28}$$

Latency at U_i is the delay in transmissions, given by

$$\ell = \frac{NT_{\rm c}}{1-\varepsilon_i}, \tag{29}$$

where $T_{\rm c}$ is the duration of a block.

C. THE SPC IN NOMA VLC SYSTEMS

In NOMA transmission strategy, the allocated block-length for U_1 and U_2 is $N_1 = N_2 = N$, since the LED transmits signal to two users simultaneously with the different power allocation. At the receiver side, the SIC is performed at U_2 to remove the interference of the U_1 message in the received signal, and then U_2 decodes its message. At U_1, the message of U_2 is treated as the interference, and U_1 directly decodes its own message in the received signal.

1) SIGNAL PROCESSING AT U_1

The signal-to-noise-plus-interference ratio (SINR) of the message signal at U_1 is given by

$$\gamma_{11} = \frac{a_1Ph_1^2}{a_2Ph_1^2+\sigma^2} = \frac{a_1}{a_2+1/\gamma_1}. \tag{30}$$

Since $\gamma_1 \in [\gamma_{\min}, \gamma_{\max}]$, then $\gamma_{11} \in \left[\gamma_{11,\min}, \gamma_{11,\max}\right] = \left[\frac{a_1}{a_2+1/\gamma_{\min}}, \frac{a_1}{a_2+1/\gamma_{\max}}\right]$. From (17) and (30), the ordered CDF of the received SINR of the message signal U_1 is given by

$$\begin{aligned}F_{\gamma_{11}}(x) &= 2\left(-\omega\left(\frac{x}{a_1-a_2x}\right)^{-\frac{1}{m+3}}+\frac{L^2}{r_{\rm c}^2}+1\right)\\ &\quad -\left(-\omega\left(\frac{x}{a_1-a_2x}\right)^{-\frac{1}{m+3}}+\frac{L^2}{r_{\rm c}^2}+1\right)^2.\end{aligned} \tag{31}$$

Power coefficients a_1 and a_2 must satisfy the condition: $a_1 - a_2x > 0$. From (26), (30) and (31), the average BLER of U_1 is approximated by

$$\bar{\varepsilon}_{11} = f\left(\gamma_{11,\max}, \gamma_{11,\min}, N_1, R_1\right). \tag{32}$$

2) SIGNAL PROCESSING AT U_2

The SIC performs to detect message signal for U_1 first, and then detect message signal for U_2. The SINR of the message signal of U_1 in U_2 is given by

$$\gamma_{21} = \frac{a_1Ph_2^2}{a_2Ph_2^2+\sigma^2} = \frac{a_1}{a_2+1/\gamma_2}. \tag{33}$$

Since $\gamma_2 \in [\gamma_{\min}, \gamma_{\max}]$, then $\gamma_{21} \in \left[\gamma_{21,\min}, \gamma_{21,\max}\right] = \left[\frac{a_1}{a_2+1/\gamma_{\min}}, \frac{a_1}{a_2+1/\gamma_{\max}}\right]$. From (17) and (33), the ordered CDF of the received SINR of the message signal of U_1 at U_2 is given by

$$F_{\gamma_{21}}(x) = \left(-\omega\left(\frac{x}{a_1-a_2x}\right)^{-\frac{1}{m+3}}+\frac{L^2}{r_{\rm c}^2}+1\right)^2. \tag{34}$$

Using (26), (33) and (34), the average BLER of U_1 at U_2 is approximated by

$$\bar{\varepsilon}_{21} = f\left(\gamma_{21,\max}, \gamma_{21,\min}, N_1, R_1\right). \tag{35}$$

The SINR of the message signal of U_2 at U_2 is given as

$$\gamma_{22} = \frac{a_2Ph_2^2}{\sigma^2} = a_2\gamma_2. \tag{36}$$

Since $\gamma_2 \in [\gamma_{\min}, \gamma_{\max}]$, then $\gamma_{22} \in \left[\gamma_{22,\min}, \gamma_{22,\max}\right] = [a_2\gamma_{\min}, a_2\gamma_{\max}]$. From (17) and (36), the ordered CDF of SINR U_2 at U_2 is given by

$$F_{\gamma_{22}}(x) = \left(-\omega\left(\frac{x}{a_2}\right)^{-\frac{1}{m+3}}+\frac{L^2}{r_{\rm c}^2}+1\right)^2. \tag{37}$$

Based on (26), the average BLER of the message U_2 at U_2 is approximated by

$$\bar{\varepsilon}_{22} = f\left(\gamma_{22,\max}, \gamma_{22,\min}, N_2, R_2\right). \tag{38}$$

The overall average BLER of U_2 is approximated by

$$\bar{\varepsilon}_2 = \bar{\varepsilon}_{21} + (1-\bar{\varepsilon}_{21})\,\bar{\varepsilon}_{22}. \tag{39}$$

D. THE SPC IN OMA VLC SYSTEMS

In OMA systems, since two users are assigned to the different orthogonal resources, there is no interference at U_1 (or U_2) caused by U_2 (or U_1). The power allocation to each user is based on the channel quality. N_1 and N_2 are the allocated block-length for U_1 and U_2, and $N_1 + N_2 = N$. At U_i ($i \in \{1, 2\}$), the SNR is given by

$$\gamma_i^{\mathrm{o}} = \frac{a_i P h_i^2}{\sigma^2} = a_i \gamma_i. \tag{40}$$

Since $\gamma_i \in [\gamma_{\min}, \gamma_{\max}]$, then $\gamma_i^{\mathrm{o}} \in \left[\gamma_{i,\min}, \gamma_{i,\max}\right] = [a_i\gamma_{\min}, a_i\gamma_{\max}]$. Following (17) and (40), the ordered CDF of the received SNR at U_i is also presented as

$$F_{\gamma_i^{\mathrm{o}}}(x) = \sum_{\hat{j}=i}^{2} \frac{2!}{(2-\hat{j})!\hat{j}!} \left(-\omega \left(\frac{x}{a_i}\right)^{-\frac{1}{m+3}} + \frac{L^2}{r_{\mathrm{c}}^2} + 1\right)^{\hat{j}} \times \left(\omega \left(\frac{x}{a_i}\right)^{-\frac{1}{m+3}} - \frac{L^2}{r_{\mathrm{c}}^2}\right)^{2-\hat{j}}. \tag{41}$$

The average BLER at U_i is approximated by

$$\bar{\varepsilon}_i^{\mathrm{o}} = f\left(\gamma_{i,\max}^{\mathrm{o}}, \gamma_{i,\min}^{\mathrm{o}}, N_i, R_i\right). \tag{42}$$

E. OPTIMAL SUM THROUGHPUT DESIGN OF THE SPC-NOMA VLC SYSTEM

In the SPC-NOMA VLC system, the transmitted signals to users are superimposed in the power domain, and the LED serves both U_1 and U_2 simultaneously in the block-length N. It is assumed that $N_1 = N_2 = N$ in NOMA systems. The goal is to obtain maximum sum throughput of the SPC-NOMA VLC system. The optimization problem is formulated as

$$\max_{R_i, a_i} \ \overline{T} \tag{43a}$$

$$\text{s.t.} \quad 0 \le a_i = 1, i \in \{1, 2\}, \tag{43b}$$

$$a_1 + a_2 = 1, \tag{43c}$$

$$0 \le R_i \le 2.56, \tag{43d}$$

where $\overline{T} = T_1 + T_2$. According to (21) and (28), the sum throughput $\overline{T}$ is formulated as

$$\overline{T} = R_1 \left(1 - Q\left(\Xi\left(\gamma_{11}, R_1\right)\right)\right) + R_2 \left(1 - Q\left(\Xi\left(\gamma_{22}, R_2\right)\right)\right)\left(1 - Q\left(\Xi\left(\gamma_{21}, R_1\right)\right)\right), \tag{44}$$

where

$$\Xi\left(\gamma_i, R_i\right) \triangleq \frac{\log_2\left(1+\gamma_i\right) - 2R_i}{\log_2 e \sqrt{2\left(1 - \frac{1}{(1+\gamma_i)^2}\right)/N}}.$$

The transmission rates R_i and power allocation coefficients a_i for U_i are determined at the LED, and the transmission rate of U_1 is independent to that of U_2. We consider the equality $a_1 + a_2 = 1$ in (43c), where total power is consumed to transmit signals to all users. According to (44), there are three variables in this optimization problem. We need to determine the power allocation and transmission rates to obtain the maximum sum throughput $\overline{T}$ subject to the constraints in (43).

Proposition 1: The error probability in (21) is monotonically decreasing with SNR/SINR.

Proof: Please see Appendix A.

According to (21) and (28), the effective throughput at each user depends on its power allocation. Following the NOMA principle, there is the trade-off between throughput and power allocation to each user. Since the Q-function is used in the throughput calculation, the optimal power allocation cannot be obtained in closed form. Therefore, the one-dimensional search is used to find the solution close to the optimal solution, where R_1 and R_2 are fixed values.

Proposition 2: The error probability in (21) is monotonically increasing with the transmission rate R_i.

Proof: Please see Appendix B.

Proposition 3: The transmission rate at each user is limited in the range [0, 2.56].

Proof: The transmission rate R is given by $R = k/N$. According to [35], the length of the information bit k of a packet is less than 256 (32 bytes) to get error probability of 10^{-5}. In SPC, the block-length N is longer than 100. Therefore, $R_i \le 2.56$. (43d) is verified.

Lemma 1: The sum throughput $\overline{T}$ does not monotonically increase with R_1 but is concave with respect to R_1.

Proof: Please see Appendix C.

Lemma 2: The sum throughput $\overline{T}$ does not monotonically increase with R_2 but is concave with respect to R_2.

Proof: Please see Appendix D.

From Appendix C and Appendix D, there exists the optimal transmission rates by solving $\frac{\partial \overline{T}}{\partial R_1} = 0$ and $\frac{\partial \overline{T}}{\partial R_2} = 0$. According (54) and (58), the optimal solutions cannot be derived in closed form. Due to three variables a_1, R_1, and R_2, we first find the optimal power allocation a_2 by one-dimension search, and then we use two-dimensional search to find the maximum sum throughput with respect to R_1 and R_2 based on the optimal power allocation coefficients derived by one-dimensional search. The optimal results are presented in the next section. We summarize the proposed algorithm to find the optimal solution in **Algorithm 1**.

The accuracy of the proposed method is dependent on the given step size τ. The complexity of the search method is $\mathcal{O}(N_I)$, where N_I is the size of the input values.

IV. NUMERICAL RESULTS

In this section, we present numerical results and utilize Monte Carlo simulations to verify the analysis in Section III. The benefits of the SPC in terms of reliability and latency are shown in the comparison between SPC and LPC in NOMA VLC systems. To demonstrate the effectiveness of the proposed system, we compare the performance of the SPC in NOMA and OMA VLC systems, and discuss the effect of the semi-angles of the LEDs to the system throughput of the SPC in the NOMA VLC system. The parameters of the channel gains are shown in Table 2. In the simulation, we choose the block-length $N_1 = N_2 = 200$, $k_1 = k_2 = 80$ bits for NOMA scheme, and $N_1 = N_2 = 100$, $k_1 = k_2 = 80$ bits for OMA scheme. In comparison of the SPC-NOMA VLC

Algorithm 1 Algorithm to Find Optimal Power Allocation and Transmission Rates

Input: Initialize vector $a_2 = 0.05 : \tau : 0.5$, with step size $\tau = 0.05$, optimal power allocation $a_2^{opt} = 0$, and maximum sum throughput $\overline{T}_{max} = 0$.

Output: $a_2^{opt}, R_1^{opt}, R_2^{opt}$

Calculate $\overline{T} \leftarrow \overline{T}(a_2)$ by (44) with fixed R_1 and R_2.

for $i \leftarrow 1$ *to length*(a_2) **do**

  Set: $\overline{T}_{samp} \leftarrow \overline{T}(i)$.

  if $\overline{T}_{samp} > \overline{T}$ **then**

    $\overline{T}_{max} \leftarrow \overline{T}_{samp}$

    $a_2^{opt} \leftarrow a_2(i)$

Set $\overline{T}_{max} \leftarrow 0$, $R_1^{opt} = 0$, $R_2^{opt} = 0$, $R_1 = 0.05 : \tau : 2.5$, and $R_2 = 0.05 : \tau : 2.5$.

Calculate $\overline{T} \leftarrow \overline{T}(R_1, R_2)$ with optimal power allocation a_2^{opt} and $a_1^{opt} = 1 - a_2^{opt}$ by (44).

for $i \leftarrow$ *length*(R_1) **do**

  for $j \leftarrow$ *length*(R_2) **do**

    Set: $\overline{T}_{samp} \leftarrow \overline{T}(i, j)$.

    if $\overline{T}_{samp} > \overline{T}_{max}$ **then**

      $\overline{T}_{max} \leftarrow \overline{T}_{samp}$

      $R_1^{opt} \leftarrow R_1(i)$

      $R_2^{opt} \leftarrow R_2(j)$

TABLE 2. Simulation parameters.

Symbol	Name of parameters	Value
L	Vertical distance from LED to circular area	2.5 m
r_c	Cell radius	3.5 m
K	Total number of users	2
$\Phi_{1/2}$	LED semi-angle	60°
Ψ_{FOV}	PD FOV	60°
R_p	PD responsibility	0.4 A/W
A	PD detection area	1 cm^2
n	Reflective index	1.5
T	Optical filter gain	1

to SPC-OMA VLC, the power allocation strategies are $a_1 = 0.8$ and $a_2 = 0.2$, and the value of SNR for the transmission is $\gamma_{Tx} = 130$ dB. The duration time of a block is $T_c = 1$ μs.

Figs. 3-10 show performances of the proposed system. In these figures, 'Ana.' and 'Sim.' denote analytical and simulation results, respectively. The analytical results are matched with the simulation results in Figs. 3-10.

In Fig. 3, we investigate the effects of the power allocation on the BLER performance of users in both NOMA and OMA systems. The analytical results match well with simulation results at different power allocation strategies. In SPC-OMA system, the BLER of U_1 is always lower than that of U_2, since there is no interference caused by another user. The BLER decreases slowly at low SNR (110-120 dB) in both two systems. At medium SNR (120-130 dB), the BLER of the SPC-NOMA system decreases quicker than that of the SPC-OMA sytem, while the BLER of the SPC-NOMA system is less than 10^{-5} at 130 dB. With $a_1 = 0.6$ and $a_2 = 0.4$, the SPC-OMA system can get the BLER

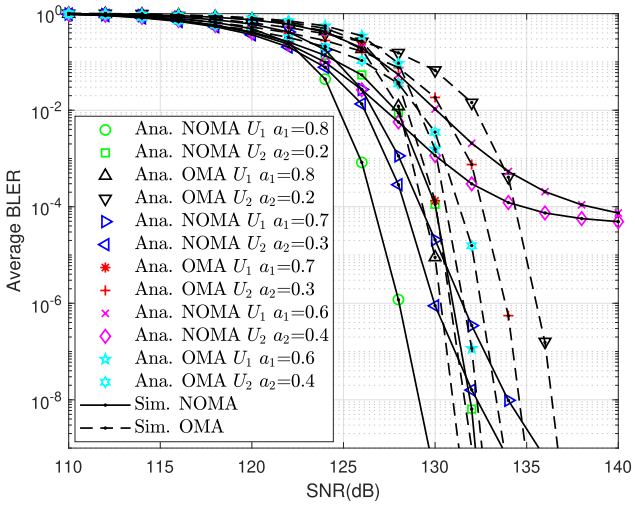

FIGURE 3. Average BLER comparison between NOMA versus OMA using SPC with different power allocation strategies.

less than 10^{-5}, while the BLER of the SPC-NOMA system cannot be less than 10^{-5}. When the power allocation for the far user increases, the BLER of the SPC-NOMA system is improved, since the interference at the near user caused by the far user in NOMA system decreases. The SPC-NOMA system can satisfy the error probability at 131 dB, while the SPC-OMA system requires 135 dB at all users. From this, the use of SPC in NOMA system requires less power than that of SPC in OMA system while increasing power to far user. Moreover, the performance of the NOMA system is enhanced when the power allocation is boosted for the far user.

In Fig. 4, we compare reliability and latency of the short packet (400 bits) and long packet (800 bits and 1000 bits) in NOMA VLC system. The reliability and latency are calculated as the function of the total block-length at $\gamma_{Tx} = 130$ dB. The reliability of short messages is higher than that of the long ones. The SPC can satisfy the reliability requirement with more than 1500 block-length while the LPC uses more than 2500 block-length to satisfy the reliability requirement. The latency of the short messages is lower than that of long ones. The use of the SPC can provide the latency in sub-millisecond while the latency of the system using the LPC is more than one millisecond. The use of the SPC can satisfy the requirements of both reliability and latency.

In Fig. 5, the reliability for U_1 is higher than that of U_2 at both NOMA and OMA systems in the range of the medium SNR. The reliability of U_2 is higher than that of U_1 at the high SNR. It shows that U_2 only obtains the high reliability when the transmitted power is high. The required SNR to fulfil the reliability of the NOMA system is lower than that of the OMA system, i.e., 130 dB for the NOMA system, and 135 dB for the OMA system. As shown in (21), the reliability of the system not only depends on the transmitted SNR but also depends on the transmission rate. In the SPC-NOMA system, the LED serves two users simultaneously with $N_1 = N_2 = N$ while the LED in the SPC-OMA VLC system serves two users in

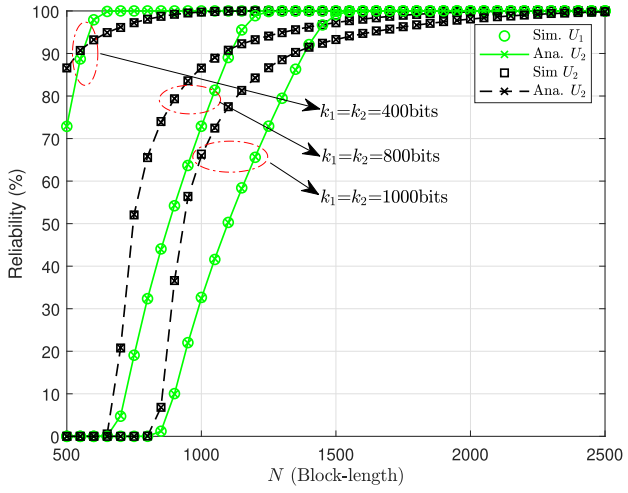

(a)

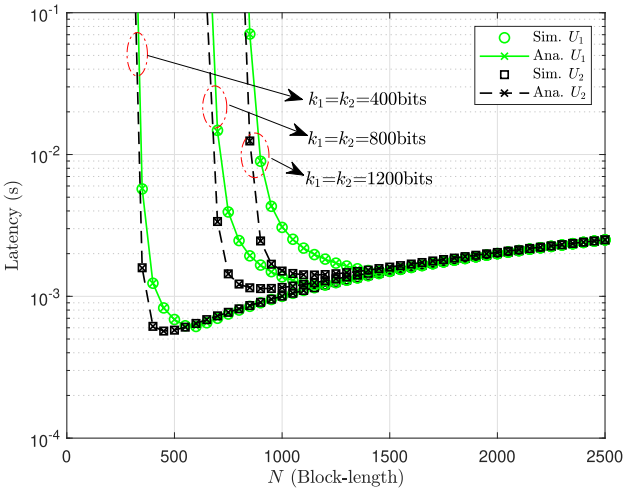

(b)

FIGURE 4. SPC and LPC for NOMA VLC.

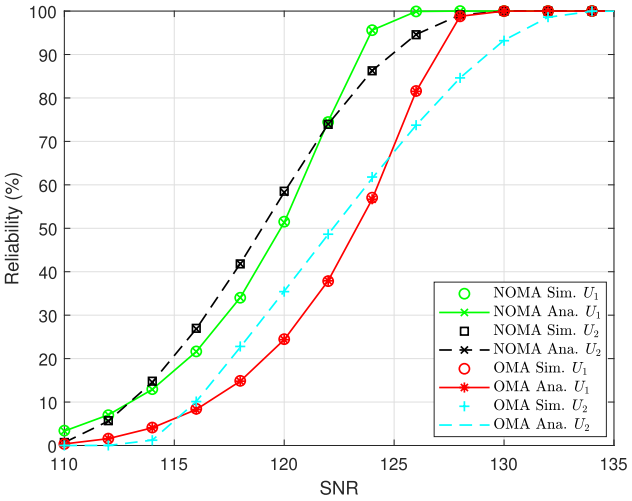

FIGURE 5. The reliability of the SPC in NOMA and OMA VLC system.

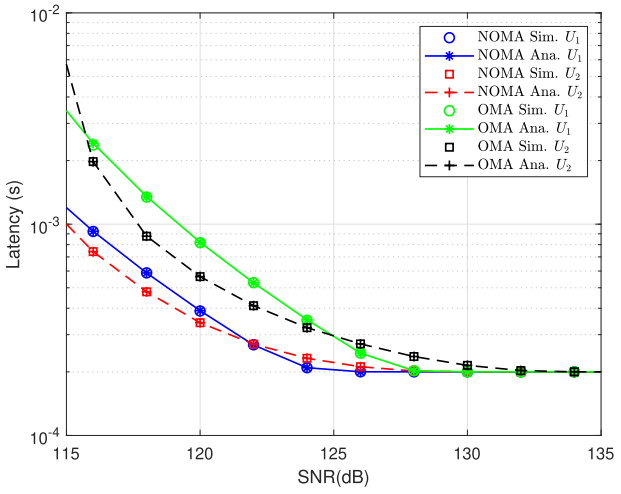

FIGURE 6. Latency comparison between NOMA versus OMA using SPC.

orthogonal time slots with $N_1 = N_2 = N/2$. The transmission rate of each user in the SPC-NOMA VLC system is always lower than that of each user in the SPC-OMA VLC system. The SPC-NOMA VLC system provides higher reliability.

In Fig. 6, the latency of SPC-NOMA users is compared to SPC-OMA users. The latency at U_2 in both NOMA and OMA VLC systems is quite similar. The latency at U_1 in NOMA system is approximately half of that at U_1 in the OMA system. The SPC-NOMA VLC system reduces latency for the users. Especially, the NOMA system fulfils the latency requirement at lower SNR than the OMA system, i.e., 116 dB for the NOMA system, and 119 dB for the OMA system.

Fig. 7 depicts sum throughput and throughput at each user of both NOMA and OMA VLC systems. The sum throughput of the NOMA system is higher than that of the OMA system. The NOMA system achieves maximum sum throughput at 130 dB while the OMA system achieves the maximum sum throughput at 134 dB. Since SIC is performed at U_2 in the NOMA system, the throughput of U_2 is higher than that of U_1 at the low SNR. At the high SNR, the far user has higher throughput. The throughput at each user depends on transmitted power, transmission rate, block-length for each user, and total block-length. All users in the NOMA system have the same block-length while the OMA system uses the block-length N to serve all users with the different allocation of total block-length for each user. The throughput of users in the NOMA schemes is higher than that of users in the OMA scheme.

Fig. 8 depicts sum throughput of the SPC in NOMA and OMA VLC schemes with various semi-angles of the LED. As shown in (13), the channel gain depends on Lambertian radiation pattern which is subject to the semi-angle of the LED. Since the sum throughput of the system depends on the channel gain, the semi-angle of the LED relates to the sum throughput. At $\gamma_{\text{Tx}} = 120$ dB, the sum throughput of the SPC-NOMA VLC system can achieve maximum at 50° semi-angle, while that of the SPC-OMA system can achieve maximum at 40° semi-angle. At $\gamma_{\text{Tx}} = 130$ dB, 35° semi-angle

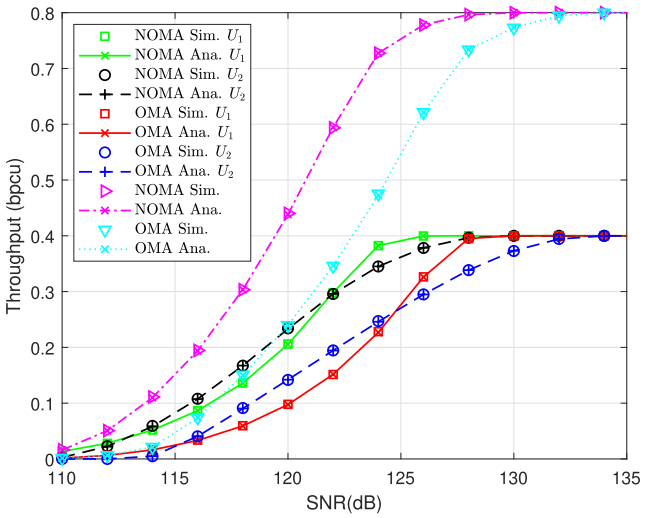

FIGURE 7. Throughput of SPC for NOMA and OMA.

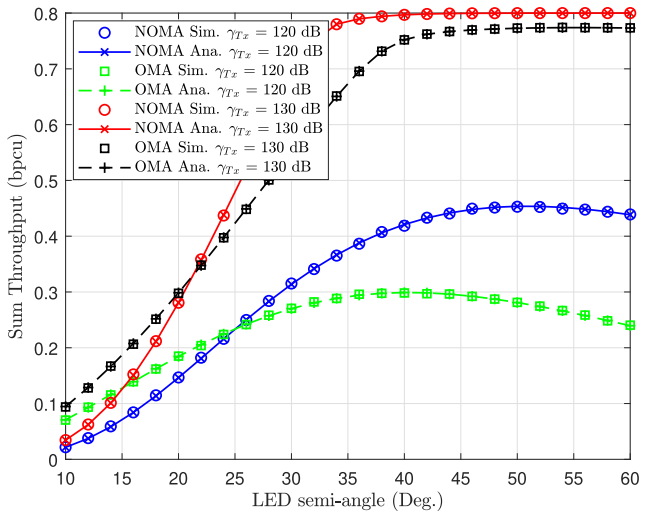

FIGURE 8. The sum throughput for different values of semi-angles at different SNR.

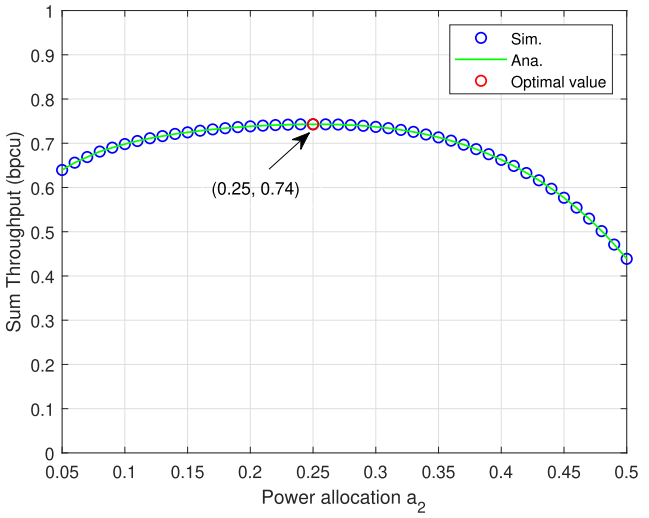

FIGURE 9. Sum throughput as the function of the power allocation for U_2 at $\gamma_{Tx} = 126$ dB, $R_1 = 0.4$, and $R_2 = 0.35$.

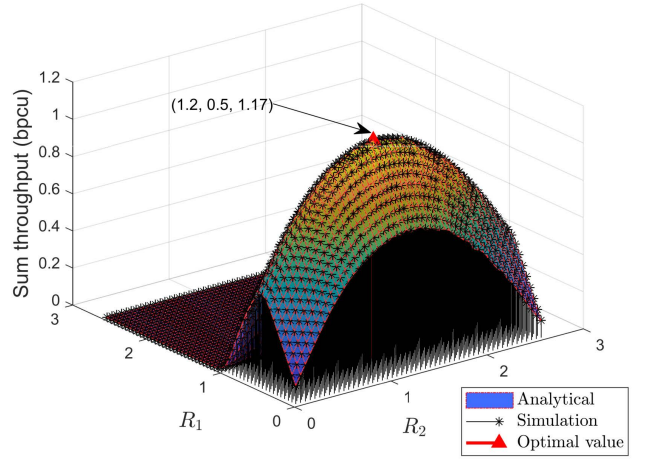

FIGURE 10. Sum throughput for the near user and the maximum throughput point $(R_2, R_1, \bar{T}) = (1.2, 0.5, 1.17)$, $\gamma_{Tx} = 126$ dB.

LED can provide the maximum sum throughput of the SPC-NOMA VLC system while the optimal semi-angle of the LED for the SPC-OMA VLC system is 45° semi-angle. The optimal semi-angle of the LED depends on the value of SNR. When we increase the value of SNR, the LED with lower semi-angle can be useful.

In Fig. 9, the optimal power allocation can be derived by using one-dimension search while keeping constant transmission rates of two users. The sum throughput increases in the range of power allocation from 0 to 0.25, and then it decreases. When the power allocation for U_2 decreases, the throughput at U_2 decreases. After obtaining optimal power allocation coefficients, the maximum sum throughputs of two users are derived by two-dimensional search. The changing values are transmission rates of two users. The result is shown in Fig. 10.

Fig. 10 depicts the impact of transmission rates on the sum throughputs. As shown in (32), (35), (38), and (39), the throughput of U_1 is independent to the throughput of the U_2. The throughput of the U_2 not only depends on R_2 but also depends on R_1. Fig. 10 shows that the sum throughput increases with R_1 in the range $R_1 \in [0, 0.5]$, and then decreases with $R_1 > 0.5$. The sum throughput increases when R_2 increases in the range $[0, 1.2]$ and then decreases with $R_2 > 1.2$. Therefore, Lemma 1 and Lemma 2 are verified. The sum throughput increases to maximum point, and then it decreases with transmission rates R_1 and R_2. It presents the trade-off between transmission rates and sum throughput of the system. According to (21), (28) and Proposition 2, the error probability is small with small values of transmission rates ($R_1 < 0.5$ and $R_2 < 1.2$), but the sum throughput is not high. Since the error probability is increasing with the transmission rates, the sum throughput decreases with the increasing of transmission rates ($R_1 > 0.5$ and $R_2 > 1.2$). Thus, this approach demonstrates that there exists a unique parameter-space position that obtains the maximum of the sum throughput.

V. CONCLUSION

In this paper, we proposed the SPC in a downlink NOMA VLC system with perfect SIC. The SPC-NOMA VLC system provides higher reliability and lower latency in comparison to the LPC-NOMA VLC systems. Moreover, the results show that the SPC-NOMA VLC system outperforms the SPC-OMA VLC system in terms of reliability, latency, and throughput. We also find out the optimal transmission rates and optimal power allocation strategy to maximize the sum throughput of the SPC-NOMA VLC system with two users. The SPC in VLC systems can support the various URLLC applications in factory automation and intelligent transportation systems.

APPENDIX A
PROOF OF PROPOSITION 1

The first partial derivative of ε_i with γ_i is given as

$$\frac{\partial \varepsilon_i}{\partial \gamma_i} = \frac{\partial}{\partial \gamma_i} Q\left(\Xi\left(\gamma_i, R_i\right)\right) = -\frac{1}{\sqrt{2\pi}} e^{-\frac{1}{2}\Xi^2(\gamma_i, R_i)} \frac{\partial \Xi\left(\gamma_i, R_i\right)}{\partial \gamma_i}, \tag{45}$$

where $\frac{\partial \Xi(\gamma_i, R_i)}{\partial \gamma_i}$ is the partial derivative of $\Xi\left(\gamma_i, R_i\right)$ with respect to γ_i, given by

$$\frac{\partial \Xi\left(\gamma_i, R_i\right)}{\partial \gamma_i} = \sqrt{N/2} \frac{1 - \ln 2 \frac{\log_2(1+\gamma_i) - 2R_i}{(1+\gamma_i)^2 - 1}}{\sqrt{(1+\gamma_i)^2 - 1}}. \tag{46}$$

It is not clear whether the partial derivative of $\Xi\left(\gamma_i, R_i\right)$ with respect to γ_i is positive or negative. Based on (46), we define a function, $H(x) = \frac{\log_2 x}{x^2-1}$. We find the range of value of $H(x)$ with $x \geq 1$ since $\gamma_i + 1 > 1$. We calculate the first derivative of $H(x)$ with respect to x, given by

$$H'(x) = \frac{h(x)}{(x^2-1)^2}, \tag{47}$$

where $h(x) = \frac{1}{\ln 2}\left(1 - \frac{1}{x}\right) - 2x \log_2 x$. Since $(x^2-1)^2 > 0$ with $x > 1$, the sign of $H(x)$ is the same as $h(x)$. The first derivative of $h(x)$ is given by

$$h'(x) = -\frac{1}{\ln 2}\left(1 - \frac{1}{x^2}\right) - 2\log_2 x. \tag{48}$$

Since $h'(x) < 0$ with $x > 1$, $h(x)$ is a decreasing function with respect to $x > 1$, and $h(x) < h(1) = 0$. $h(x)$ is negative with $x > 1$, and then $H'(x) < 0$ with $x > 1$, which means that $H(x)$ is also a decreasing function with respect to $x > 1$. We determine the value range of $H(x)$ by using L'Hospital's rule, as $\lim_{x\to 1} H(x) = \frac{1}{2\ln 2}$ and $\lim_{x\to\infty} H(x) = 0$. Since $R_i \geq 0$ and $\gamma_i > 0$, we have

$$\begin{aligned} 1 - \ln 2 \frac{\log_2\left(1+\gamma_i\right) - 2R_i}{(1+\gamma_i)^2 - 1} &\geq 1 - \ln 2 \frac{\log_2\left(1+\gamma_i\right)}{(1+\gamma_i)^2 - 1} \\ &= 1 - \ln 2\, H\left(1+\gamma_i\right) \\ &> 1 - \ln 2 \frac{1}{2\ln 2} = \frac{1}{2} > 0. \end{aligned} \tag{49}$$

Since $\frac{\partial \Xi(\gamma_i, R_i)}{\partial \gamma_i} > 0$, $\frac{\partial \varepsilon_i}{\partial \gamma_i} < 0$. Therefore, it can be concluded that ε_i is decreasing function with respect to γ_i.

APPENDIX B
PROOF OF PROPOSITION 2

The first partial derivative of ε_i with R_i is given as

$$\frac{\partial}{\partial R_i} Q\left(\Xi\left(\gamma_i, R_i\right)\right) = -\frac{1}{\sqrt{2\pi}} e^{-\frac{1}{2}\Xi^2(\gamma_i, R_i)} \frac{\partial \Xi\left(\gamma_i, R_i\right)}{\partial R_i}, \tag{50}$$

where

$$\frac{\partial \Xi\left(\gamma_i, R_i\right)}{\partial R_i} = -\frac{2}{\log_2 e \sqrt{2\left(1 - \frac{1}{(1+\gamma_i)^2}\right)/N}} = -\Theta\left(\gamma_i\right). \tag{51}$$

Then, $\frac{\partial}{\partial R_i} Q\left(\Xi\left(\gamma_i, R_i\right)\right)$ in (50) can be expressed as

$$\frac{\partial}{\partial R_i} Q\left(\Xi\left(\gamma_i, R_i\right)\right) = \frac{1}{\sqrt{2\pi}} e^{-\frac{1}{2}\Xi^2(\gamma_i, R_i)} \Theta\left(\gamma_i\right). \tag{52}$$

Since $\Theta\left(\gamma_i\right) \geq 0$, $\frac{\partial}{\partial R_i} Q\left(\Xi\left(\gamma_i, R_i\right)\right) \geq 0$. It can be concluded that ε_i is an increasing function with respect to R_i.

APPENDIX C
PROOF OF LEMMA 1

To determine the optimal value of R_1 which maximizes $\overline{T}$, we examine the monotonicity and concavity of $\overline{T}$ with respect to R_1. The first and second derivatives of $\overline{T}$ are examined as below.

Following (44), the first derivative of $\overline{T}$ is given by

$$\begin{aligned} \frac{\partial \overline{T}}{\partial R_1} &= 1 - Q\left(\Xi\left(\gamma_{11}, R_1\right)\right) - R_1 \frac{\partial}{\partial R_1} Q\left(\Xi\left(\gamma_{11}, R_1\right)\right) \\ &\quad - R_2\left(1 - Q\left(\Xi\left(\gamma_{22}, R_2\right)\right)\right) \frac{\partial}{\partial R_1} Q\left(\Xi\left(\gamma_{21}, R_1\right)\right). \end{aligned} \tag{53}$$

By substituting (52) into (53), the first derivative of $\overline{T}$ with respect to R_1 is given by

$$\begin{aligned} \frac{\partial \overline{T}}{\partial R_1} &= 1 - Q\left(\Xi\left(\gamma_{11}, R_1\right)\right) - R_1 \frac{1}{\sqrt{2\pi}} \Theta\left(\gamma_{11}\right) e^{-\frac{1}{2}\Xi^2(\gamma_{11}, R_1)} \\ &\quad - R_2\left(1 - Q\left(\Xi\left(\gamma_{22}, R_2\right)\right)\right) \frac{1}{\sqrt{2\pi}} \Theta\left(\gamma_{21}\right) e^{-\frac{1}{2}\Xi^2(\gamma_{21}, R_1)}. \end{aligned} \tag{54}$$

Since the value of (54) is not always positive or negative, $\overline{T}$ is not an increasing or decreasing function with respect to R_1. Next, we examine the monotonicity of $\overline{T}$ with respect to R_1. Following (54), the second derivative of $\overline{T}$ with respect to R_1 is given by

$$\begin{aligned} \frac{\partial^2 \overline{T}}{\partial R_1^2} &= -\frac{\partial}{\partial R_1} Q\left(\Xi\left(\gamma_{11}, R_1\right)\right) - \frac{1}{\sqrt{2\pi}} \Theta\left(\gamma_{11}\right) e^{-\frac{1}{2}\Xi^2(\gamma_{11}, R_1)} \\ &\quad - R_1 \frac{1}{\sqrt{2\pi}} \Theta\left(\gamma_{11}\right) \frac{\partial}{\partial R_1} e^{-\frac{1}{2}\Xi^2(\gamma_{11}, R_1)} \\ &\quad - R_2\left(1 - Q\left(\Xi\left(\gamma_{22}, R_2\right)\right)\right) \frac{1}{\sqrt{2\pi}} \Theta\left(\gamma_{21}\right) \end{aligned}$$

$$\times \frac{\partial}{\partial R_1} e^{-\frac{1}{2}\Xi^2(\gamma_{21},R_1)}. \quad (55)$$

Using (51) and (52), (55) is presented as

$$\begin{aligned}\frac{\partial^2 \overline{T}}{\partial R_1^2} = &-\frac{2}{\sqrt{2\pi}}\Theta(\gamma_{11})\, e^{-\frac{1}{2}\Xi^2(\gamma_{11},R_1)} \\ &-R_1 \frac{1}{\sqrt{2\pi}}\Theta^2(\gamma_{11})\,\Xi(\gamma_{11},R_1)\, e^{-\frac{1}{2}\Xi^2(\gamma_{11},R_1)} \\ &-R_2\left(1-Q\left(\Xi(\gamma_{22},R_2)\right)\right)\frac{1}{\sqrt{2\pi}}\Theta^2(\gamma_{21}) \\ &\times \Xi(\gamma_{21},R_1)\, e^{-\frac{1}{2}\Xi^2(\gamma_{21},R_1)}. \end{aligned} \quad (56)$$

Since $\Xi(\gamma_i, R_i) \geq 0$ and $\Theta(\gamma_i) \geq 0$, then $\frac{\partial^2 \overline{T}}{\partial R_1^2} \leq 0$. We can conclude that $\overline{T}$ is the concave function with respect to R_1. Therefore, the optimal R_1 can be derived by solving $\frac{\partial \overline{T}}{\partial R_1} = 0$.

APPENDIX D
PROOF OF LEMMA 2

To find out the existence of the optimal transmission rate R_2 that maximizes $\overline{T}$, the monotonicity and concavity are examined by deriving the first and second derivatives of $\overline{T}$ with respect to R_2, presented as following.

From (44), the first derivative of $\overline{T}$ with respect to R_2 is given by

$$\begin{aligned}\frac{\partial \overline{T}}{\partial R_2} = &\left(1-Q\left(\Xi(\gamma_{22},R_2)\right)-R_2\frac{\partial}{\partial R_2}Q\left(\Xi(\gamma_{22},R_2)\right)\right) \\ &\times\left(1-Q\left(\Xi(\gamma_{21},R_1)\right)\right). \end{aligned} \quad (57)$$

By substituting (52) into (57), we have

$$\begin{aligned}\frac{\partial \overline{T}}{\partial R_2} = &\left(1-Q\left(\Xi(\gamma_{22},R_2)\right)-R_2\frac{1}{\sqrt{2\pi}}\Theta(\gamma_{22})\right. \\ &\left.\times e^{-\frac{1}{2}\Xi^2(\gamma_{22},R_2)}\right)\times\left(1-Q\left(\Xi(\gamma_{21},R_1)\right)\right). \end{aligned} \quad (58)$$

Since the value $\frac{\partial \overline{T}}{\partial R_2}$ is not always positive or negative, $\overline{T}$ is not an increasing or decreasing function with respect to R_2. Then, we examine the second derivative of $\overline{T}$ with respect to R_2. From (58), we have

$$\begin{aligned}\frac{\partial^2 \overline{T}}{\partial R_2^2} = &\left(-\frac{\partial}{\partial R_2}Q\left(\Xi(\gamma_{22},R_2)\right)-\frac{1}{\sqrt{2\pi}}\Theta(\gamma_{22})\right. \\ &\times e^{-\frac{1}{2}\Xi^2(\gamma_{22},R_2)} \\ &\left.-R_2\frac{1}{\sqrt{2\pi}}\Theta(\gamma_{22})\frac{\partial}{\partial R_2}e^{-\frac{1}{2}\Xi^2(\gamma_{22},R_2)}\right)\Big) \\ &\times\left(1-Q\left(\Xi(\gamma_{21},R_1)\right)\right)\Big). \end{aligned} \quad (59)$$

By substituting (51) and (52) into (59), we have

$$\begin{aligned}\frac{\partial^2 \overline{T}}{\partial R_2^2} = &\left(-\frac{2}{\sqrt{2\pi}}\Theta(\gamma_{22})\, e^{-\frac{1}{2}\Xi^2(\gamma_{22},R_2)}-R_2\frac{1}{\sqrt{2\pi}}\Theta^2(\gamma_{22})\right. \\ &\left.\times\Xi(\gamma_{22},R_2)\, e^{-\frac{1}{2}\Xi^2(\gamma_{22},R_2)}\right)\Big)\times\left(1-Q\left(\Xi(\gamma_{21},R_1)\right)\right). \end{aligned} \quad (60)$$

Since $\Xi(\gamma_i, R_i) \geq 0$ and $\Theta(\gamma_i) \geq 0$, $\frac{\partial^2 \overline{T}}{\partial R_2^2} \leq 0$. Therefore, the sum throughput $\overline{T}$ is the concave function with respect to R_2. The optimal R_2 can be obtained by solving $\frac{\partial \overline{T}}{\partial R_2} = 0$.

REFERENCES

[1] J. G. Andrews, S. Buzzi, W. Choi, S. V. Hanly, A. Lozano, A. C. K. Soong, and J. C. Zhang, "What will 5G be?" *IEEE J. Sel. Areas Commun.*, vol. 32, no. 6, pp. 1065–1082, Jun. 2014.
[2] S. Wu, H. Wang, and C. H. Youn, "Visible light communications for 5G wireless networking systems: From fixed to mobile communications," *IEEE Netw.*, vol. 28, no. 6, pp. 41–45, Nov./Dec. 2014.
[3] S. Idris, U. Mohammed, J. Sanusi, and S. Thomas, "Visible light communication: A potential 5G and beyond communication technology," in *Proc. 15th Int. Conf. Electron., Comput. Comput. (ICECCO)*, Abuja, Nigeria, Dec. 2019, pp. 1–6.
[4] H. Yang, W.-D. Zhong, C. Chen, and A. Alphones, "Integration of visible light communication and positioning within 5G networks for Internet of Things," *IEEE Netw.*, vol. 34, no. 5, pp. 134–140, Sep. 2020.
[5] X. Liu, X. Wei, L. Guo, Y. Liu, Q. Song, and A. Jamalipour, "Turning the signal interference into benefits: Towards indoor self-powered visible light communication for IoT devices in industrial radio-hostile environments," *IEEE Access*, vol. 7, pp. 24978–24989, 2019.
[6] C. Du, F. Zhang, S. Ma, Y. Tang, H. Li, H. Wang, and S. Li, "Secure transmission for downlink NOMA visible light communication networks," *IEEE Access*, vol. 7, pp. 65332–65341, 2019.
[7] C. She, C. Sun, Z. Gu, Y. Li, C. Yang, H. V. Poor, and B. Vucetic, "A tutorial on ultrareliable and low-latency communications in 6G: Integrating domain knowledge into deep learning," *Proc. IEEE*, vol. 109, no. 3, pp. 204–246, Mar. 2021.
[8] Y. Polyanskiy, H. V. Poor, and S. Verdú, "Channel coding rate in the finite blocklength regime," *IEEE Trans. Inf. Theory*, vol. 56, no. 5, pp. 2307–2359, May 2010.
[9] I. Parvez, A. Rahmati, I. Guvenc, A. I. Sarwat, and H. Dai, "A survey on low latency towards 5G: RAN, core network and caching solutions," *IEEE Commun. Surveys Tuts.*, vol. 20, no. 4, pp. 3098–3130, 4th Quart. 2018.
[10] C. E. Shannon, "A mathematical theory of communication," *Bell Syst. Tech. J.*, vol. 27, no. 3, pp. 379–423, Jul. 1948.
[11] G. Durisi, T. Koch, and P. Popovski, "Toward massive, ultrareliable, and low-latency wireless communication with short packets," *Proc. IEEE*, vol. 104, no. 9, pp. 1711–1726, Sep. 2016.
[12] Y. Yu, H. Chen, Y. Li, Z. Ding, and B. Vucetic, "On the performance of non-orthogonal multiple access in short-packet communications," *IEEE Commun. Lett.*, vol. 22, no. 3, pp. 590–593, Mar. 2018.
[13] W. Yang, G. Durisi, T. Koch, and Y. Polyanskiy, "Quasi-static multiple-antenna fading channels at finite blocklength," *IEEE Trans. Inf. Theory*, vol. 60, no. 7, pp. 4232–4265, Jul. 2014.
[14] A. Karimi, K. I. Pedersen, N. H. Mahmood, G. Pocovi, and P. Mogensen, "Efficient low complexity packet scheduling algorithm for mixed URLLC and eMBB traffic in 5G," in *Proc. IEEE 89th Veh. Technol. Conf. (VTC-Spring)*, Kuala Lumpur, Malaysia, Apr. 2019, pp. 1–6.
[15] L. Dai, B. Wang, Y. Yuan, S. Han, I. Chih-Lin, and Z. Wang, "Non-orthogonal multiple access for 5G: Solutions, challenges, opportunities, and future research trends," *IEEE Commun. Mag.*, vol. 53, no. 9, pp. 74–81, Sep. 2015.
[16] J. So and Y. Sung, "Improving non-orthogonal multiple access by forming relaying broadcast channels," *IEEE Commun. Lett.*, vol. 20, no. 9, pp. 1816–1819, Sep. 2016.
[17] M. Mohammadi, X. Shi, B. K. Chalise, Z. Ding, H. A. Suraweera, C. Zhong, and J. S. Thompson, "Full-duplex non-orthogonal multiple access for next generation wireless systems," *IEEE Commun. Mag.*, vol. 57, no. 5, pp. 110–116, May 2019.
[18] Y. Liu, Z. Qin, M. Elkashlan, Y. Gao, and L. Hanzo, "Enhancing the physical layer security of non-orthogonal multiple access in large-scale networks," *IEEE Trans. Wireless Commun.*, vol. 16, no. 3, pp. 1656–1672, Mar. 2017.
[19] Z. Ding, F. Adachi, and H. V. Poor, "The application of MIMO to non-orthogonal multiple access," *IEEE Trans. Wireless Commun.*, vol. 15, no. 1, pp. 537–552, Jan. 2016.
[20] Y. Song, W. Yang, Z. Xiang, N. Sha, H. Wang, and Y. Yang, "An analysis on secure millimeter wave NOMA communications in cognitive radio networks," *IEEE Access*, vol. 8, pp. 78965–78978, 2020.
[21] M. R. Amini and M. W. Baidas, "Performance analysis of URLL energy-harvesting cognitive-radio IoT networks with short packet and diversity transmissions," *IEEE Access*, vol. 9, pp. 79293–79306, 2021.
[22] J. Chen, L. Yang, and M.-S. Alouini, "Physical layer security for cooperative NOMA systems," *IEEE Trans. Veh. Technol.*, vol. 67, no. 5, pp. 4645–4649, May 2018.

[23] A. Al-Dweik, Y. Iraqi, K.-H. Park, M. Al-Jarrah, E. Alsusa, and M.-S. Alouini, "Efficient NOMA design without channel phase information using amplitude-coherent detection," *IEEE Trans. Commun.*, early access, Oct. 13, 2021, doi: 10.1109/TCOMM.2021.3119368.
[24] Y. Iraqi and A. Al-Dweik, "Power allocation for reliable SIC detection of rectangular QAM-based NOMA systems," *IEEE Trans. Veh. Technol.*, vol. 70, no. 8, pp. 8355–8360, Aug. 2021.
[25] Z. Ding, Y. Liu, J. Choi, Q. Sun, M. Elkashlan, I. Chih-Lin, and H. V. Poor, "Application of non-orthogonal multiple access in LTE and 5G networks," *IEEE Commun. Mag.*, vol. 55, no. 2, pp. 185–191, Feb. 2017.
[26] C. Chen, S. Fu, X. Jian, M. Liu, X. Deng, and Z. Ding, "NOMA for energy-efficient LiFi-enabled bidirectional IoT communication," *IEEE Trans. Commun.*, vol. 69, no. 3, pp. 1693–1706, Mar. 2021.
[27] R. C. Kizilirmak, C. R. Rowell, and M. Uysal, "Non-orthogonal multiple access (NOMA) for indoor visible light communications," in *Proc. 4th Int. Workshop Opt. Wireless Commun. (IWOW)*, Sep. 2015, pp. 98–101.
[28] Y. Fu, Y. Hong, L. Chen, and C. W. Sung, "Enhanced power allocation for sum rate maximization in OFDM-NOMA VLC systems," *IEEE Photon. Technol. Lett.*, vol. 30, no. 13, pp. 1218–1221, Jul. 1, 2018.
[29] L. Yin, W. O. Popoola, X. Wu, and H. Haas, "Performance evaluation of non-orthogonal multiple access in visible light communication," *IEEE Trans. Commun.*, vol. 64, no. 12, pp. 5162–5175, Dec. 2016.
[30] B. Makki, T. Svensson, and M. Zorzi, "Finite block-length analysis of the incremental redundancy HARQ," *IEEE Wireless Commun. Lett.*, vol. 3, no. 5, pp. 529–532, Oct. 2014.
[31] M. B. Janjua, D. B. da Costa, and H. Arslan, "User pairing and power allocation strategies for 3D VLC-NOMA systems," *IEEE Wireless Commun. Lett.*, vol. 9, no. 6, pp. 866–870, Jun. 2020.
[32] D. D. Wackerly, W. Mendenhall, and R. L. Scheaffer, *Mathematical Statistics With Applications*. Pacific Grove, CA, USA: Duxbury Press, 1996.
[33] Z. Ding, Z. Yang, P. Fan, and H. V. Poor, "On the performance of non-orthogonal multiple access in 5G systems with randomly deployed users," *IEEE Signal Process. Lett.*, vol. 21, no. 12, pp. 1501–1505, Dec. 2014.
[34] M. Abramowitz and I. A. Stegun, Eds., *Handbook of Mathematical Functions With Formulas, Graphs, and Mathematical Tables*, 10th ed. Washington, DC, USA: U.S. Government Printing Office, 1972.
[35] M. Shirvanimoghaddam, M. S. Mohammadi, R. Abbas, A. Minja, C. Yue, B. Matuz, G. Han, Z. Lin, W. Liu, Y. Li, S. Johnson, and B. Vucetic, "Short block-length codes for ultra-reliable low latency communications," *IEEE Commun. Mag.*, vol. 57, no. 2, pp. 130–137, Feb. 2019.

GIANG N. TRAN (Graduate Student Member, IEEE) received the B.S. degree from the Advanced Program in Electrical Engineering, Thai Nguyen University of Technology, Vietnam, in 2019. He is currently pursuing the combined M.S. and Ph.D. degree with the Department of Electrical, Electronic and Computer Engineering, University of Ulsan, South Korea. His main research interests include ultra-reliable and low-latency communication, 5G communication, and visible light communication.

SUNGHWAN KIM (Member, IEEE) received the B.S., M.S., and Ph.D. degrees from Seoul National University, South Korea, in 1999, 2001, and 2005, respectively. He was a Postdoctoral Visitor at the Georgia Institute of Technology (GeorgiaTech), from 2005 to 2007, and a Senior Engineer at Samsung Electronics, from 2007 to 2011. He is currently a Professor at the Department of Electrical, Electronic and Computer Engineering, University of Ulsan, South Korea. His main research interests include channel coding, modulation, massive MIMO, visible light communication, quantum information, and storage systems.